Physics Contribution

Shortening Delivery Times of Intensity Modulated Proton Therapy by Reducing Proton Energy Layers During Treatment Plan Optimization

CrossMark

Steven van de Water, MSc, * **Hanne M. Kooy, PhD,** †
Ben J.M. Heijmen, PhD, * **and Mischa S. Hoogeman, PhD** *

*Department of Radiation Oncology, Erasmus MC Cancer Institute, Rotterdam, The Netherlands; and
†F. H. Burr Proton Therapy Center, Department of Radiation Oncology, Massachusetts General Hospital and Harvard Medical School, Boston, Massachusetts*

Summary

We developed a method to reduce the number of energy layers in robust IMPT treatment plans without compromising dosimetric plan quality. This resulted in an average energy layer reduction of 45% for oropharyngeal cases and 28% for prostate cases. When assuming 1, 2, or 5 seconds energy switching time, the delivery time per fraction was on average shortened by 25%, 32%, or 38% for oropharyngeal cases, and by 16%, 20%, or 24% for prostate cases.

Purpose: To shorten delivery times of intensity modulated proton therapy by reducing the number of energy layers in the treatment plan.

Methods and Materials: We have developed an energy layer reduction method, which was implemented into our in-house-developed multicriteria treatment planning system "Erasmus-iCycle." The method consisted of 2 components: (*1*) minimizing the logarithm of the total spot weight per energy layer; and (*2*) iteratively excluding low-weighted energy layers. The method was benchmarked by comparing a robust "time-efficient plan" (with energy layer reduction) with a robust "standard clinical plan" (without energy layer reduction) for 5 oropharyngeal cases and 5 prostate cases. Both plans of each patient had equal robust plan quality, because the worst-case dose parameters of the standard clinical plan were used as dose constraints for the time-efficient plan. Worst-case robust optimization was performed, accounting for setup errors of 3 mm and range errors of 3% + 1 mm. We evaluated the number of energy layers and the expected delivery time per fraction, assuming 30 seconds per beam direction, 10 ms per spot, and 400 Giga-protons per minute. The energy switching time was varied from 0.1 to 5 seconds.

Results: The number of energy layers was on average reduced by 45% (range, 30%-56%) for the oropharyngeal cases and by 28% (range, 25%-32%) for the prostate cases. When assuming 1, 2, or 5 seconds energy switching time, the average delivery

time was shortened from 3.9 to 3.0 minutes (25%), 6.0 to 4.2 minutes (32%), or 12.3 to 7.7 minutes (38%) for the oropharyngeal cases, and from 3.4 to 2.9 minutes (16%), 5.2 to 4.2 minutes (20%), or 10.6 to 8.0 minutes (24%) for the prostate cases.

Conclusions: Delivery times of intensity modulated proton therapy can be reduced substantially without compromising robust plan quality. Shorter delivery times are likely to reduce treatment uncertainties and costs. © 2015 Elsevier Inc. All rights reserved.

Introduction

A reduction of the delivery time per fraction is likely to have a beneficial effect on patient comfort, treatment uncertainties, and treatment costs. Especially the last 2 motives are important for intensity modulated proton therapy (IMPT). Compared with photon therapy, IMPT is relatively sensitive to treatment uncertainties (1, 2), and it is associated with higher treatment costs (3, 4).

In spot-scanned IMPT, each proton pencil beam (or "spot") is spatially characterized by its lateral position and its position in depth, the latter depending on the energy of the proton beam. Spots are delivered one by one, adjusting the lateral position and/or energy in between the delivery of each spot. In modern commercial double-scanning proton delivery systems (ie systems in which the proton beam is magnetically deflected in both lateral directions), the energy switching time is typically in the order of seconds, causing it to be the major component of the delivery time (5). A reduction of the number of energy layers in an IMPT treatment plan is therefore likely to result in a reduction of the delivery time. However, reducing energy layers by simply increasing the energy layer spacing was demonstrated to result in a worsening of the plan quality (6, 7).

In this study we hypothesized that the number of energy layers can be reduced without affecting the plan quality, because of the degeneracy of IMPT treatment planning. Some treatment plans with a comparable plan quality may contain many energy layers, whereas others contain fewer. By taking the number of energy layers into account during treatment planning (which is typically not done), the solution can potentially be steered toward an outcome with fewer energy layers. For CyberKnife treatment planning, a similar approach resulted in treatment plans with fewer principal beam directions, thereby reducing delivery times in robotic radiosurgery (8).

The aim of this study was to reduce the delivery time per fraction of robust IMPT treatment plans without compromising the dosimetric plan quality. To this purpose, we developed a method to incorporate the reduction of energy layers in the treatment planning process. This method was implemented into our treatment planning system and tested by generating robust treatment plans for 5 patients with oropharyngeal cancer and 5 patients with locally advanced prostate cancer.

Methods and Materials

Treatment planning system

The novel energy layer reduction method was implemented into our in-house-developed treatment planning system "Erasmus-iCycle" (7, 9). The planning system does not optimize a single objective function that is the weighted sum of all objectives, but it performs "prioritized" or "lexicographic" multi-criteria optimization instead. This means that objectives are optimized one by one according to their priorities, which are defined a priori by the user in the so-called "wish list." Generally, a single wish list can be used per patient group, which enables fully automatic treatment planning. Automatic plan generation allows for an objective comparison between different planning strategies and was shown to result in superior plan quality compared with manual planning (10, 11).

Erasmus-iCycle features two planning methods for IMPT, which are schematically illustrated in Figure 1. First, treatment plans can be generated using the traditional planning method in which the candidate spots are distributed over the target volume using a regular grid with a spot spacing defined by the user (denoted as "regular grid planning"). Second, treatment planning can be performed using the new and more efficient "pencil beam resampling" method, as described by Van de Water et al (7). This method uses an iterative approach in which the multi-criteria optimization is performed repeatedly, while adding in each iteration a new sample of randomly selected candidate spots to the obtained solution. The user has to define the sample size and a stopping criterion to terminate the iterative resampling process. Pencil beam resampling was shown to reduce optimization times by a factor of 2.8 to 5.6 on average, compared with traditional regular grid planning (7).

In Erasmus-iCycle both planning methods feature a "spot reduction" loop (indicated in Fig. 1). After each multi-criteria optimization, low-weighted spots and spots with a weight below the minimum deliverable spot weight are iteratively excluded from the solution, while constraining previously achieved dose parameters. The exclusion of spots is terminated when further reduction results in a violation of previously achieved dose parameters. In this way Erasmus-iCycle will always generate deliverable plans that are efficient in terms of the number of spots (7).
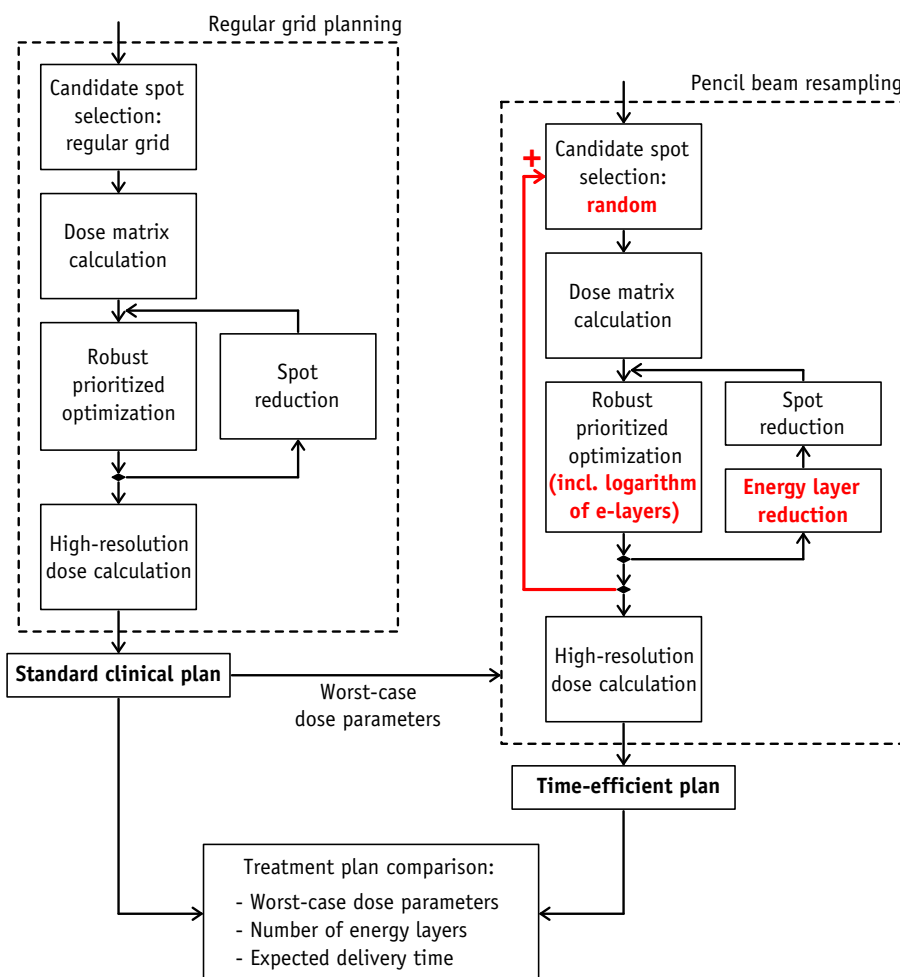
Fig. 1.   Study workflow describing treatment plan generation and comparison. The differences between the standard clinical plan and the time-efficient plan are highlighted in red. A color version of this figure is available at www.redjournal.org.

The treatment planning system also features a robust planning mode to generate IMPT treatment plans that are robust against setup errors and range errors. Erasmus-iCycle uses a "minimax" approach for this purpose (12, 13). The nominal scenario and several error scenarios are simultaneously included in the multi-criteria optimization, optimizing the worst scenario for each objective. In this study, robust optimization was performed using a total of 9 scenarios: the nominal scenario (1 scenario), 3-mm setup errors in positive and negative directions along 3 axes (6 scenarios), and a proton undershoot and overshoot of 3% + 1 mm (2 scenarios).

The proton dose calculation algorithm used for IMPT treatment planning was developed at the Massachusetts General Hospital and Harvard Medical School, where it is implemented in their in-house-developed radiotherapy platform "ASTROID" (14). The algorithm accounts for density heterogeneities using a superposition–convolution approach. In this study we used a dose grid with $3 \times 3 \times 3\text{-mm}^3$ resolution. Available proton energies ranged from 70 to 230 MeV, with corresponding beam widths ranging from 7 to 3 mm σ (in-air at the isocenter), respectively. A range shifter of 75 mm water-equivalent thickness could be

inserted during the delivery of a field. The minimum deliverable spot weight was 0.001 Giga-protons.

Energy layer reduction method

The energy layer reduction method that we developed in this study consisted of 2 components. The first component was the introduction of an additional objective, which aimed at minimizing the logarithm of the total spot weight per energy layer. The logarithm has a steeper gradient at lower values, causing the optimizer to focus on the minimization of spot weights in low-weighted energy layers, thereby redistributing them to relatively high-weighted energy layers. The second component was the iterative exclusion of low-weighted energy layers, which was implemented as an extension of the spot reduction loop described above. After each multi-criteria optimization, low-weighted energy layers were excluded from the solution first, before switching to the iterative exclusion of individual spots. The energy layer reduction was terminated when further exclusion resulted in the violation of previously achieved dose parameters. Excluded energy layers

were not available during candidate spot selection in subsequent resampling iterations.

Patient data and dose prescription

Data of 5 patients with oropharyngeal cancer and 5 patients with locally advanced prostate cancer were used in this study. The oropharyngeal cases (3 unilateral and 2 bilateral cases) were prescribed a simultaneously integrated boost of 66 Gy to the primary tumor and positive neck levels, and 54 Gy to the elective neck levels, delivered in 30 fractions. The median high-dose clinical target volume (CTV) was 41 mL (range, 5-106 mL), whereas the median total high-dose and low-dose CTV was 95 mL (range, 67-229 mL). The prostate cases were prescribed a simultaneously integrated boost of 74 Gy to the prostate expanded by a margin of 4 mm, and 55 Gy to the seminal vesicles and pelvic lymph nodes, both expanded using a margin of 7 mm. These margins were applied to construct an internal target volume (ITV), to account for the organ-specific interfraction motion in prostate cases (15). The median high-dose ITV was 60 mL (range, 56-65 mL), and the median total high-dose and low-dose ITV was 875 mL (range, 810-957 mL).

The wish lists containing the constraints and objectives for both patient groups are given in the Supplementary Material (available online at www.redjournal.org). The constraints and objectives of the target volumes were chosen such that the volume receiving 95% of the prescribed dose was higher than 99% ($V_{95\%} > 99\%$) and the volume receiving 107% of the prescribed dose was smaller than 2% ($V_{107\%} < 2\%$) in all error scenarios included in the optimization. For the oropharyngeal cases, we included the salivary glands, spinal cord, brainstem, larynx, oral cavity, and swallowing muscles as organs at risk (OARs) in the robust optimization, whereas the rectum, bladder, and femur heads were considered for the prostate cases. The oropharyngeal cases were planned using a 3-beam arrangement (gantry angles: 60°, 180°, and 300°), whereas the prostate cases were planned using a 2-beam arrangement (gantry angles: 90° and 270°) (15, 16).

Study design

To assess the effectiveness of the proposed energy layer reduction method, we compared for each patient a robust "time-efficient" IMPT plan with a robust "standard clinical" IMPT plan. The study workflow is depicted in Figure 1. First, the standard clinical plan was generated using traditional regular grid planning without energy layer reduction, resembling clinical practice in currently operating proton facilities. Regular grid planning was performed using a lateral spot spacing of 7 mm, corresponding to approximately 2 times the width (σ) of the smallest spot (6). The spacing between energy layers depended on the proton energy and was set to the longitudinal width of the

Bragg peak (at 80% of the peak height) (6, 17). Second, the time-efficient plan was generated using the new pencil beam resampling method with energy layer reduction. The worst-case dose parameters of each objective achieved in the standard clinical plan were used as dose constraints for the time-efficient plan, to ensure comparable robust plan quality in both treatment plans. Pencil beam resampling was performed using a sample size of 5000 spots per iteration, which were randomly selected from a grid with 1-mm lateral spot spacing and the same energy layer spacing as used for the standard clinical plan. Time-efficient plan generation was terminated when the number of energy layers could not be reduced any further in 2 consecutive resampling iterations.

We compared the worst-case dose parameters of the CTVs (oropharyngeal cases), ITVs (prostate cases), and OARs, considering all 9 scenarios included in the robust optimization. Next to that, we evaluated the number of energy layers and the expected delivery time per fraction (ie time between the delivery of the first spot and the last spot, excluding patient setup), which was calculated assuming 30 seconds per beam direction (gantry rotation and beam setup), 10 ms per spot (lateral spot adjustment), and 400 Giga-protons per minute (beam current). The energy switching time was varied between 0.1 and 5 seconds, because this was assumed to cover the variety in currently operating spot-scanning systems, from the PSI Gantry 2 to a slow-switching system, respectively (18, 19). Switching times of 1, 2, and 5 seconds were assumed to be typical values for commercial systems and are therefore explicitly mentioned in this article.

Results

Table 1 lists the plan parameters of the standard clinical plans and the time-efficient plans for the oropharyngeal cases and the prostate cases. For both patient groups, the table shows that the worst-case dose parameters were nearly identical, indicating comparable robust plan quality for both types of treatment plans. The number of energy layers in the time-efficient treatment plans was on average reduced by 45% (range, 30%-56%) for the oropharyngeal cases and by 28% (range, 25%-32%) for the prostate cases, compared with the standard clinical plans. The corresponding delivery times per fraction are depicted in Figure 2 as a function of the energy switching time. When assuming energy switching times of 1, 2, or 5 seconds, the average delivery time of the oropharyngeal cases was shortened from 3.9 to 3.0 minutes (25%; range, 18%-30%), from 6.0 to 4.2 minutes (32%; range, 22%-39%), or from 12.3 to 7.7 minutes (38%; range, 26%-48%). For the prostate cases, the delivery time was reduced from 3.4 to 2.9 minutes (16%; range, 12%-19%), from 5.2 to 4.2 minutes (20%; range, 17%-23%), or from 10.6 to 8.0 minutes (24%; range, 21%-27%) on average, when assuming energy switching times of 1, 2, or 5 seconds, respectively. The

Table 1   Average worst-case dose parameters and delivery parameters (and range) for the standard clinical plans and the time-efficient plans of the oropharyngeal and prostate cases. Estimated delivery times are listed for energy switching times of 1, 2, or 5 seconds

Parameter	Value	Standard clinical plan	Time-efficient plan	Relative difference (%)
Oropharyngeal cases (n=5)				
CTV-low	$V_{95\%}$ (%)	99.5 (99.3-99.7)	99.6 (99.4-99.8)	0 (0-0)
CTV-high	$V_{95\%}$ (%)	99.4 (99.0-99.8)	99.5 (99.3-99.8)	0 (0-0)
CTV-high	$V_{107\%}$ (%)	0.3 (0.1-0.7)	0.3 (0.1-0.7)	31 (−40 to 113)
Parotid glands	Mean (Gy)	14.1 (6.9-27.0)	14.1 (7.0-27.0)	0 (0-2)
Submandibular glands	Mean (Gy)	34.7 (12.3-59.6)	34.7 (12.4-59.6)	0 (−1 to 0)
Spinal cord	Max (Gy)	20.7 (19.7-21.3)	20.3 (19.6-20.9)	−2 (−4 to 0)
Brainstem	Max (Gy)	19.4 (18.3-20.4)	19.4 (18.2-20.6)	0 (−10 to 13)
Larynx	Mean (Gy)	18.0 (8.7-33.9)	18.0 (8.7-33.7)	0 (−1 to 0)
Oral cavity	Mean (Gy)	19.5 (6.8-32.7)	19.5 (6.8-32.7)	0 (−1 to 0)
Swallowing muscles	Mean (Gy)	23.9 (13.6-34.4)	23.8 (13.1-34.7)	−1 (−3 to 1)
CI-low		2.23 (1.99-2.48)	2.20 (1.93-2.43)	−2 (−3 to 0)
CI-high		2.19 (1.98-2.41)	2.13 (1.98-2.31)	−2 (−4 to 0)
Beam directions		3 (3-3)	3 (3-3)	0 (0-0)
Energy layers		126 (107-144)	71 (52-100)	−45 (−56 to −30)
Spots		2099 (1123-3314)	1809 (1050-2841)	−12 (−18 to −7)
Total spot weight	(Gp)	3899 (2046-6411)	3855 (2069-6298)	−1 (−3 to 1)
Delivery time (1 s)	(min)	3.9 (3.5-4.5)	3.0 (2.6-3.6)	−25 (−30 to −18)
Delivery time (2 s)	(min)	6.0 (5.3-6.9)	4.2 (3.4-5.3)	−32 (−39 to −22)
Delivery time (5 s)	(min)	12.3 (10.6-14.1)	7.7 (6.1-10.3)	−38 (−48 to −26)
Prostate cases (n=5)				
ITV-low	$V_{95\%}$ (%)	99.3 (99.1-99.4)	99.3 (99.1-99.4)	0 (0-0)
ITV-high	$V_{95\%}$ (%)	99.3 (98.7-99.7)	99.5 (98.8-99.8)	0 (0-0)
ITV-high	$V_{107\%}$ (%)	0.1 (0.0-0.1)	0.1 (0.0-0.3)	29 (−67 to 190)
Femur left	Max (Gy)	50.9 (50.5-51.3)	50.8 (50.2-51.3)	0 (−2 to 0)
Femur right	Max (Gy)	50.3 (48.7-51.0)	50.2 (47.8-51.1)	0 (−2 to 1)
Rectum	Mean (Gy)	26.3 (16.3-38.9)	26.2 (16.3-38.9)	0 (0-0)
Bladder	Mean (Gy)	39.2 (34.1-43.6)	39.2 (34.1-43.6)	0 (0-0)
Femur left	Mean (Gy)	27.9 (20.9-31.8)	27.9 (20.9-31.8)	0 (0-0)
Femur right	Mean (Gy)	30.9 (27.9-35.5)	30.9 (27.9-35.6)	0 (0-0)
CI-low		1.61 (1.55-1.69)	1.62 (1.56-1.71)	1 (0-1)
CI-high		1.54 (1.51-1.59)	1.56 (1.51-1.59)	1 (−1 to 3)
Beam directions		2 (2-2)	2 (2-2)	0 (0-0)
Energy layers		107 (101-112)	77 (72-83)	−28 (−32 to −25)
Spots		3835 (3445-4360)	3649 (3069-4300)	−5 (−15 to 8)
Total spot weight	(Gp)	8326 (7867-9056)	8169 (7777-8839)	−2 (−2 to −1)
Delivery time (1 s)	(min)	3.4 (3.3-3.5)	2.9 (2.7-3.1)	−16 (−19 to −12)
Delivery time (2 s)	(min)	5.2 (4.9-5.4)	4.2 (3.9-4.5)	−20 (−23 to −17)
Delivery time (5 s)	(min)	10.6 (10.0-11.0)	8.0 (7.5-8.6)	−24 (−27 to −21)

Abbreviations: CI-high = high-dose conformity index; CI-low = low-dose conformity index; CTV = clinical target volume; CTV/ITV-high = high-dose target volume; CTV/ITV-low = low-dose target volume; Gp = Giga-protons; ITV = internal target volume.

The conformity index was defined as the patient volume receiving 95% of the prescription dose divided by the target volume (CTV or ITV).

(field-specific) plan parameters of each individual patient are provided in the Supplementary Material (available online at www.redjournal.org).

The worst-case dose−volume histograms of both treatment plans for 1 oropharyngeal case and 1 prostate case are displayed in Figure 3. The worst-case dose−volume histograms were constructed by taking for each dose−volume point the worst value from the 9 scenarios included in the optimization (nominal, 3-mm setup errors, 3% + 1-mm range errors). The curves are generally located very close to each other, indicating a good agreement between the standard clinical plans and the time-efficient plans. Figure 4 shows for both cases the corresponding total dose

distributions and the doses per field for the nominal scenario. The total dose distributions of the standard clinical plans and the time-efficient plans were very similar, especially for the oropharyngeal case. Larger differences can be observed in the dose distributions of the individual fields, illustrating the degeneracy of IMPT treatment plans. For the oropharyngeal case, the intensity of the individual fields could differ between both types of plans. For the prostate case, a change in the spatial distribution can be observed, indicating a redistribution of the spots within the remaining energy layers in the time-efficient plan.

The total spot weight per energy layer is depicted in Figure 5 for the same cases as shown in Figures 3 and 4.
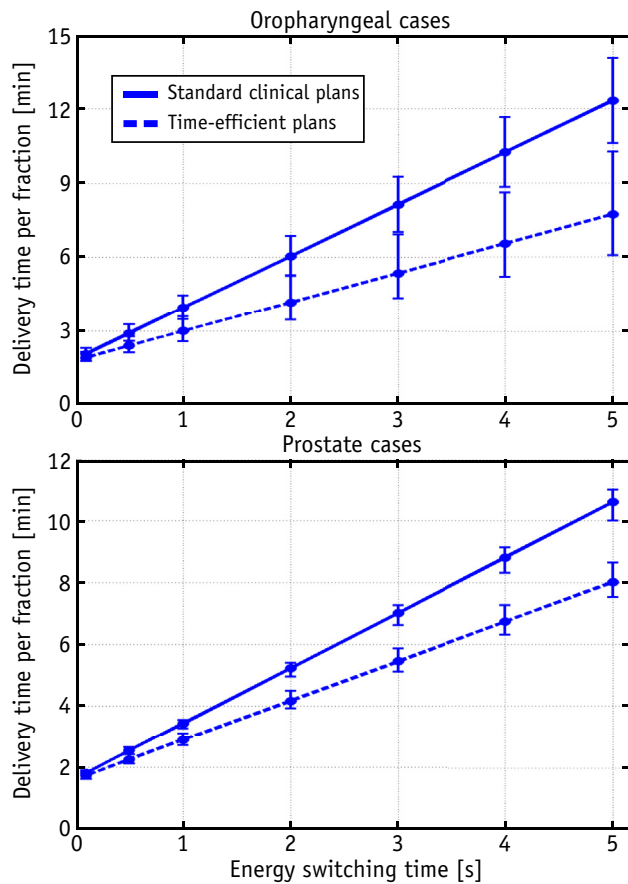
Fig. 2. Average delivery time as a function of the energy switching time for standard clinical plans (solid lines) and time-efficient plans (dashed lines). Whiskers indicate minimum and maximum values.

The energy layer reduction method generally resulted in a redistribution of spots from low-weighted energy layers to high-weighted energy layers, which was observed most strongly for the oropharyngeal case. The graphs show that the energy layers were not excluded evenly from all beam directions or uniformly across the proton energy range. Furthermore, the excluded low-weighted energy layers did not necessarily correspond to low proton energies, as illustrated by beam 3 of the oropharyngeal case.

Discussion

This study shows that the number of energy layers in robust IMPT treatment plans can be reduced considerably without affecting the dosimetric plan quality. This can result in a substantial shortening of the delivery time.

It should be noted that the delivery times reported in this study did not include the time required for patient setup. The relative gain in overall treatment efficiency will therefore depend on the patient setup time and on the number of treatment rooms that share the proton beam. In multi-room centers, patient setup can take place while patients in other treatment rooms are irradiated. If patient
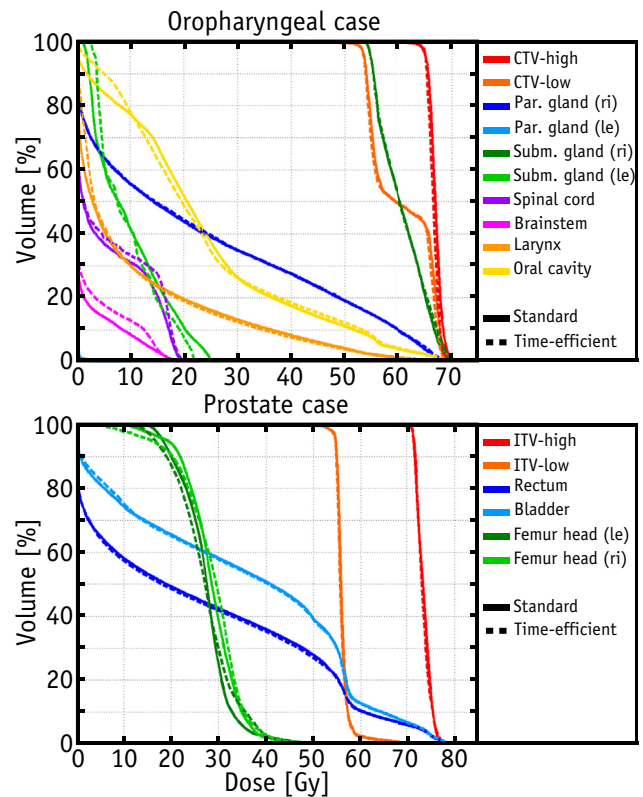

Fig. 3. Worst-case dose–volume histograms for the standard clinical plan (solid lines) and the time-efficient plan (dashed lines) of 1 oropharyngeal case and 1 prostate case. Histograms depict the worst-case value for each dose–volume point. CTV = clinical target volume; ITV = internal target volume.

setup can be completed within the delivery time in other rooms, a shortening of the delivery time will reduce the beam waiting time and enable more efficient use of multiple treatment rooms. This can result in an increase in the number of treated patients and subsequently in a reduction of treatment costs. Regardless of the type of facility, delivery time reduction may also improve patient comfort and reduce treatment uncertainties, because intrafraction displacements of, for example, spine, prostate, and liver tumors tend to increase with delivery time (20-23).

Very recently, Cao et al (24) published an alternative method to reduce energy layers in IMPT treatment plans. They proposed a mixed-integer programming approach, iteratively reducing the number of energy layers until the plan quality degraded beyond a user-defined level. The number of energy layers in nonrobust IMPT treatment plans was reduced by 14% to 19% for prostate cases, by 11% for a lung case, and by 26% for a mesothelioma case, when allowing for the cost-function value to worsen by 5%. Our study shows that energy layer reduction can also be performed for robust IMPT treatment plans and without compromising dosimetric plan quality. The larger energy layer reduction observed in this study (25%-56% vs 11%-26% by Cao et al) might be explained by differences between both methods or by
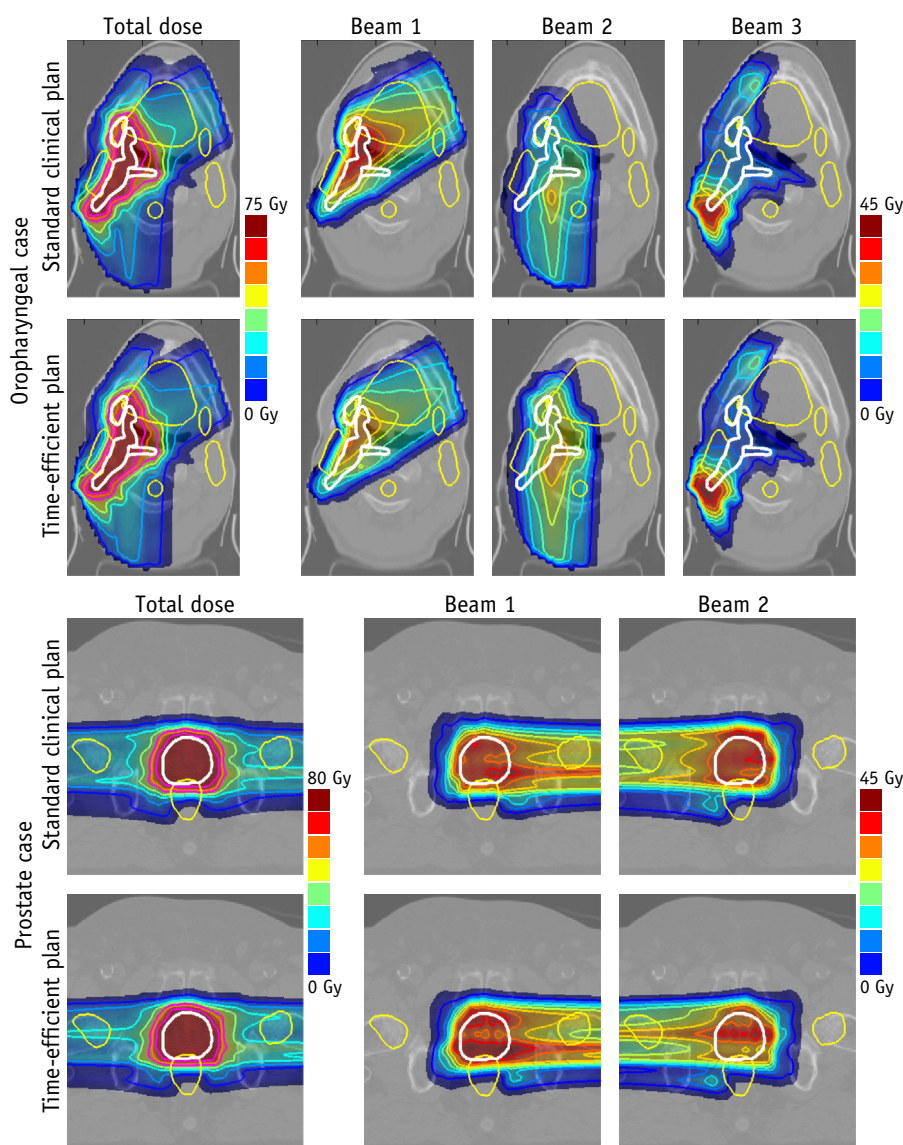
Fig. 4. Dose distributions (total and per field) for the oropharyngeal and prostate cases depicted in Figure 3. The clinical target volume/internal target volume is delineated in white and organs at risk in yellow. The 95% prescription isodose lines (low-dose and high-dose) are indicated in pink. A color version of this figure is available at www.redjournal.org.

differences in patient and plan characteristics. More details on the performance of the different components of our method are provided in the Supplementary Material (available online at www.redjournal.org).

A reduction of the number of energy layers can also be achieved by an enlargement of the energy layer spacing, but this was shown to compromise plan quality (6, 7). We verified this for one oropharyngeal case by generating a standard clinical plan using an energy layer spacing increased by a factor of 2. The lateral spot spacing was reduced to keep the total number of optimized spots approximately the same. This resulted in an energy layer reduction (50%) that was comparable to the reduction in the time-efficient plan of this patient (52%). However, worst-case doses in the submandibular glands were increased by

7.1 Gy (+33%, mean dose), in the spinal cord by 3.3 Gy (+17%, maximum dose), in the larynx by 13.0 Gy (+149%, mean dose), in the oral cavity by 5.2 Gy (+30%, mean dose), and in the swallowing muscles by 12.1 Gy (+68%, mean dose), compared with the time-efficient plan.

These results confirm that energy layers cannot be excluded before the start of treatment planning without compromising plan quality. Energy layer reduction should be incorporated in the planning process, because it makes use of the interchangeability of spots within and between the applied beam directions. This might also explain why fewer energy layers were excluded in the prostate cases. For these patients, it is more difficult to exchange spots between beam directions, because the pelvic lymph nodes on either side of the patient were mainly irradiated from a
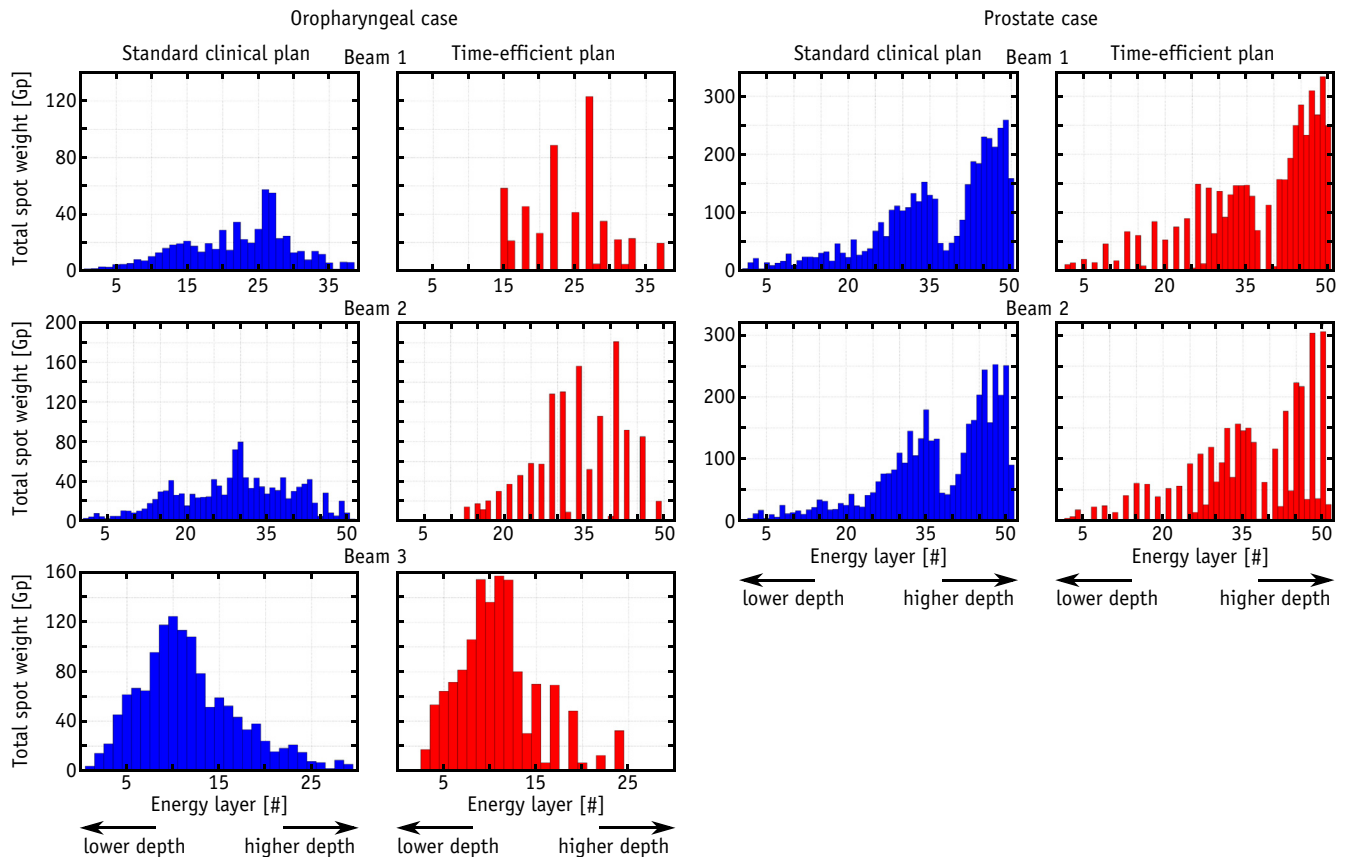
Fig. 5.   Total spot weight per energy layer for each beam direction of the standard clinical plan (blue) and the time-efficient plan (red) of the oropharyngeal and prostate cases depicted in Figures 3 and 4. A color version of this figure is available at www.redjournal.org.

single beam direction to spare centrally located OARs. The effect of other patient and plan characteristics (eg tumor size, tissue heterogeneities, beam directions) on the performance of energy layer reduction should be investigated in future research.

The number of energy layers was incorporated in the mathematical optimization by means of the logarithm of the total spot weight per energy layer. However, the logarithm is a concave function, and this can give problems during optimization. As a consequence, it required 16.7 hours on average to complete the fully automated energy layer reduction. It would therefore be useful to find a convex function to include the number of energy layers in the mathematical optimization.

Conclusions

The number of energy layers in robust IMPT treatment plans can be reduced considerably without affecting the dosimetric plan quality. The method presented in this study resulted in an average energy layer reduction of 45% and 28% for oropharyngeal and prostate cases, respectively. When assuming 1, 2, or 5 seconds energy switching time, the delivery time was on average shortened by 25%, 32%, or 38% for the oropharyngeal cases, and by 16%, 20%, or 24% for the prostate cases. Shorter delivery times are likely to reduce treatment uncertainties and costs.

References

1. Lomax AJ. Intensity modulated proton therapy and its sensitivity to treatment uncertainties 1: The potential effects of calculational uncertainties. *Phys Med Biol* 2008;53:1027-1042.
2. Lomax AJ. Intensity modulated proton therapy and its sensitivity to treatment uncertainties 2: The potential effects of inter-fraction and inter-field motions. *Phys Med Biol* 2008;53:1043-1056.
3. Goitein M, Jermann M. The relative costs of proton and x-ray radiation therapy. *Clin Oncol* 2003;15:S37-S50.
4. Peeters A, Grutters JPC, Pijls-Johannesma M, et al. How costly is particle therapy? Cost analysis of external beam radiotherapy with carbon-ions, protons and photons. *Radiother Oncol* 2010;95:45-53.
5. Schippers JM, Lomax AJ. Emerging technologies in proton therapy. *Acta Oncol* 2011;50:838-850.
6. Hillbrand M, Georg D. Assessing a set of optimal user interface parameters for intensity-modulated proton therapy planning. *J Appl Clin Med Phys* 2010;11:93-104.
7. Van de Water S, Kraan AC, Breedveld S, et al. Improved efficiency of multi-criteria IMPT treatment planning using iterative resampling of randomly placed pencil beams. *Phys Med Biol* 2013;58:6969-6983.

8. Van de Water S, Hoogeman MS, Breedveld S, et al. Shortening treatment time in robotic radiosurgery using a novel node reduction technique. *Med Phys* 2011;38:1397-1405.

9. Breedveld S, Storchi PRM, Voet PWJ, et al. iCycle: Integrated, multicriterial beam angle, and profile optimization for generation of coplanar and noncoplanar IMRT plans. *Med Phys* 2012;39:951-963.

10. Voet PWJ, Dirkx MLP, Breedveld S, et al. Toward fully automated multicriterial plan generation: A prospective clinical study. *Int J Radiat Oncol Biol Phys* 2013;85:866-872.

11. Voet PWJ, Dirkx MLP, Breedveld S, et al. Fully automated volumetric modulated arc therapy plan generation for prostate cancer patients. *Int J Radiat Oncol Biol Phys* 2014;88:1175-1179.

12. Fredriksson A, Forsgren A, Hårdemark B. Minimax optimization for handling range and setup uncertainties in proton therapy. *Med Phys* 2011;38:1672-1684.

13. Chen W, Unkelbach J, Trofimov A, et al. Including robustness in multi-criteria optimization for intensity-modulated proton therapy. *Phys Med Biol* 2012;57:591.

14. Kooy HM, Clasie BM, Lu H-M, et al. A Case Study in Proton Pencil-Beam Scanning Delivery. *Int J Radiat Oncol Biol Phys* 2010;76:624-630.

15. Thörnqvist S, Muren LP, Bentzen L, et al. Degradation of target coverage due to inter-fraction motion during intensity-modulated proton therapy of prostate and elective targets. *Acta Oncol* 2013;52:521-527.

16. Van de Water TA, Lomax AJ, Bijl HP, et al. Using a reduced spot size for intensity-modulated proton therapy potentially improves salivary gland−sparing in oropharyngeal cancer. *Int J Radiat Oncol Biol Phys* 2012;82:e313-e319.

17. Kang JH, Wilkens JJ, Oelfke U. Non-uniform depth scanning for proton therapy systems employing active energy variation. *Phys Med Biol* 2008;53:N149-N155.

18. Safai S, Bula C, Meer D, et al. Improving the precision and performance of proton pencil beam scanning. *Transl Cancer Res* 2012;1:196-206.

19. Flanz J, Bortfeld T. Evolution of technology to optimize the delivery of proton therapy: The third generation. *Semin Radiat Oncol* 2013;23:142-148.

20. Hoogeman MS, Nuyttens JJ, Levendag PC, et al. Time dependence of intrafraction patient motion assessed by repeat stereoscopic imaging. *Int J Radiat Oncol Biol Phys* 2008;70:609-618.

21. Langen KM, Willoughby TR, Meeks SL, et al. Observations on real-time prostate gland motion using electromagnetic tracking. *Int J Radiat Oncol Biol Phys* 2008;71:1084-1090.

22. Mutanga TF, de Boer HCJ, Rajan V, et al. Day-to-day reproducibility of prostate intrafraction motion assessed by multiple kV and MV imaging of implanted markers during treatment. *Int J Radiat Oncol Biol Phys* 2012;83:400-407.

23. von Siebenthal M, Székely G, Lomax AJ, et al. Systematic errors in respiratory gating due to intrafraction deformations of the liver. *Med Phys* 2007;34:3620-3629.

24. Cao W, Lim G, Liao L, et al. Proton energy optimization and reduction for intensity-modulated proton therapy. *Phys Med Biol* 2014;59:6341-6354.